ScieRxiv

NOT PEER-REVIEWED

Research Article

Rapid design of high-strength high-conductivity copper alloys based on machine learning and NSGA-II multi-objective optimization integrated strategy

Yuhong Li[1], Jing Xu[1], Bo Guan[1,*], Dan Wu[1], Yushuai Han[1], Xiankang Pan[1], Huadi Xu[1], Zhi Hu[2*], Guohong Ma[2], Qiang Hu[1,*]

[1]Jiangxi Key Laboratory of Advanced Copper-based Materials, Institute of Materials and Intelligent Manufacturing, Jiangxi Academy of Sciences, Nanchang 330096, Jiangxi, China.

[2]School of Advanced Manufacturing, Nanchang University, Nanchang 330031, Jiangxi, China.

***Correspondence to:** Dr. Bo Guan, Dr. Qiang Hu, Jiangxi Key Laboratory of Advanced Copper-based Materials, Institute of Materials and Intelligent Manufacturing, Jiangxi Academy of Sciences, Nanchang 330096, Jiangxi, China. Email: bguan2022@163.com;huqiang1225@163.com; Dr. Zhi Hu, School of Advanced Manufacturing, Nanchang University, Nanchang 330031, Jiangxi, China. Email: huzhi@ncu.edu.cn

Received: 08 July 2026 | Approved: 07 August 2026 | Online: 07 August 2026

Abstract

The high-strength and high-conductivity properties of Cu-Ni-Si alloys are synergistically regulated by composition and thermomechanical processing. However, the global design within the multi-dimensional composition-processing space faces dual challenges: high dimensional complexity and strength- conductivity performance trade-offs. To address these issues, this study proposes a novel paradigm for rapid alloy design that integrates

machine learning, multi-objective optimization, and empirical knowledge: First, a gradient boosting regression (GBR) surrogate model is constructed and embedded with the NSGA-II multi-objective optimization algorithm to efficiently generate the Pareto front in the six-dimensional Ni-Co-Si-Mg-Ag-Cr composition space. Then, based on previous process development experience, the multi-pass rolling and aging process is fixed within an optimal window, forming a stepwise strategy of composition optimization coupled with fixed processing parameters. Through composition screening, an outstanding Cu-0.65Ni-1.65Co-0.44Si-0.09Mg-0.46Ag copper alloy was successfully designed using only seven sets of experiments, achieving a tensile strength of 868.63 MPa and a conductivity of 59.2% IACS. While maintaining the reported high strength level, this alloy significantly improves its electrical conductivity, breaking through the performance bottleneck of existing high-strength and high-conductivity copper alloys and demonstrating excellent application potential. Furthermore, the synergistic mechanism by which trace Ag promotes the formation of nanoscale δ-$(Ni,Co)_2Si$ precipitates and purifies solutes in the matrix is systematically elucidated. The intrinsic mechanism underlying precipitate strengthening and simultaneous improvement of strength and conductivity through composition design is revealed, providing a new perspective for the composition design of precipitation-strengthened alloys.

Keywords: Cu-Ni-Co-Si-Mg-Ag alloy, machine learning, multi-objective optimization

INTRODUCTION

In high-end manufacturing fields such as current 5G communications, integrated circuit lead frames, and high-voltage connectors for new energy vehicles, conductive materials are undergoing a paradigm shift from single-performance optimization to synergistic breakthroughs in “ultra-high strength and high conductivity”. As a typical precipitation-strengthened copper alloy, Cu-Ni-Si alloys have become core candidates to replace expensive and toxic beryllium copper (C17200)[1,2] and performance-limited copper-iron alloys (C19400)[3-5], owing to their advantage of achieving tensile strength exceeding 800 MPa while maintaining relatively high electrical conductivity(45~50%IACS). However, although existing commercial grades such as C70250[6-8] and C70350[9-12] have achieved a preliminary balance between strength and electrical conductivity, the surging computing power demand brought by the development and deployment of large models,

together with the application scenarios of high-current connectors for new energy high-voltage platforms, has imposed more stringent performance requirements on high-strength and high-conductivity copper alloys used in power transmission systems. The composition ratios of traditional Cu-Ni-Si alloys have approached their physical properties limits. How to rapidly and accurately design alloys that meet the target performance within a multi-dimensional composition space has become the key to breaking through material bottlenecks and supporting the development of next-generation power electronic devices.

In recent years, the combination of machine learning and multi-objective optimization has become an important approach for alloy composition design. For example, Zhang *et al.* designed a Cu-1.3Ni-1.4Co-0.56Si-0.03Mg alloy based on machine learning and Bayesian multi-objective optimization, achieving a tensile strength of 858 MPa and an electrical conductivity of 47.6 %IACS[13]. Li *et al.* developed a Cu-2.1Ni-0.80Co-0.74Si-0.22Mg-0.11Ti alloy with a tensile strength of 911.4 MPa and an electrical conductivity of 44.37 %IACS[15]. Based on a comprehensive literature review[16], it is found that existing high-strength and high-conductivity Cu-Ni-Si alloys suffer from a prominent strength-conductivity trade-off bottleneck: when the tensile strength exceeds 800 MPa, the electrical conductivity generally fails to break through 50 %IACS. This is mainly because traditional high-strength copper alloys rely on strengthening mechanisms such as solid-solution strengthening and grain refinement strengthening, which inevitably lead to a decrease in electrical conductivity. Given that both existing literature[9,13,14,17] have confirmed that elements such as Cr, Mg, and Ag can synergistically improve the comprehensive strength-conductivity performance of copper alloys. However, it is of great significance to precisely identify the optimal composition combination in the six-dimensional Ni-Co-Si-Mg-Ag-Cr composition space, so as to achieve a substantial increase in electrical conductivity while maintaining high strength.

Meanwhile, given that Cu-Ni-Si alloys are typical age-hardening alloys, rolling and aging processes are also crucial for the synergistic regulation of strength and conductivity, in addition to chemical composition. In general, both properties can be improved simultaneously as the number of rolling-aging passes increases: alternating multi-pass rolling and aging can significantly increase the density of second-phase particles, which

would contribute to reducing the electron scattering caused by solute atoms in the matrix, thereby optimizing electrical conductivity. However, incorporating all complex process parameters (solution temperature/duration, hot rolling temperature, total rolling reduction, *etc.*) into machine learning models will drastically increase the feature dimension and training difficulty, leading to higher model complexity and greater prediction uncertainty. Accordingly, this paper proposes an integrated design strategy: on the basis of previous research, composition optimization is realized using machine learning and multi-objective optimization, while the thermomechanical processing route adopts the optimized multi-pass rolling- aging scheme previously established by our team[14,18]. First, a GBR surrogate model is embedded into the NSGA- II multi-objective optimization algorithm to efficiently search for optimal solutions in the six-dimensional composition space, aiming to significantly improve electrical conductivity while maintaining high strength. Process parameters are fixed within the optimal multi-pass rolling-aging window based on previous research foundations. This strategy enables the successful design of a high-strength and high-conductivity copper alloy with a tensile strength of 868.63 MPa and a conductivity of 59.2 %IACS through only seven rounds of experimental verification, providing a reliable approach for the efficient and rapid design of cu alloys.

METHODS

Overall design strategy

To achieve rapid and efficient design of copper alloy compositions with enhanced precipitation hardening properties, this study employs a strategy comprising “data-driven analysis, model building, intelligent optimization, and experimental validation”. First, a comprehensive dataset of copper alloys is curated; next, a machine learning prediction model is constructed; subsequently, the NSGA-II algorithm[18] is used to identify the pareto-optimal solution set; and finally, the design results are validated through experimental fabrication and multiscale characterization. The complete technical workflow is illustrated in the Figure 1.

(1) Copper alloy data collection: The effectiveness of machine learning depends on data quality. With reference to the dataset sizes reported in literature on machine learning-aided design of copper alloys, this study systematically constructed a high-quality dataset

containing 412 preprocessed copper alloy records, covering typical alloy systems such as Cu-Ni-Si, Cu-Ni-Co-Si-Mg, Cu-Cr, and Cu-Ag, which represents a reasonable scale for the design field[19-22]. Input features include the mass fractions of six elements—Ni, Co, Si, Mg, Ag, and Cr—as well as the processing sequence (solution treatment → first rolling → first aging → second rolling → second aging). The output targets are tensile strength and electrical conductivity.

(2) Machine learning model development: To improve model accuracy and physical interpretability, material descriptors such as second ionization energy and atomic radius were incorporated[13-14]. The optimal combination of alloying elements was identified through exhaustive screening using a random forest algorithm. Subsequently, a multidimensional feature space was constructed by integrating chemical composition, alloying elements, and process parameters. Hyperparameters were optimized via grid search and cross-validation, and various machine learning algorithms were compared. Ultimately, Gradient Boosted Regression (GBR)[24] was identified as the optimal model for predicting UTS and EC.

(3) NSGA-II multi-objective optimization: After constructing the best-performing predictive model, the NSGA-II algorithm was used to find the pareto-optimal solution set. To further improve the quality of the solution set, Bayesian optimization was introduced to optimize key hyperparameters (population size, crossover probability, mutation probability, and PM distribution index). With the objective of minimizing the negative hypervolume[25], the optimal combination of hyperparameters was determined after 150 iterations (each iteration comprising 300 generations of evolutionary search). Subsequently, a full evolutionary search of 3,000 generations was performed using the optimal parameters, outputting a solution set that fully covers the pareto front.

(4) Experimental validation and microstructural characterization: From the output set of Pareto solutions, a constraint on the (Ni+Co)/Si ratio (4.0~5.4) was applied, and performance thresholds of UTS ≥ 850 MPa and EC ≥ 50% IACS were set to screen out seven representative compositions for smelting and preparation. Following multi-step thermomechanical treatment, the mechanical properties and electrical conductivity were systematically tested; among these, three representative alloys (containing Cr, containing

Ag, and containing Cr-Ag) underwent further multi-scale characterization via SEM, EBSD, XRD, and TEM to reveal the intrinsic relationship between composition, microstructure, and properties.

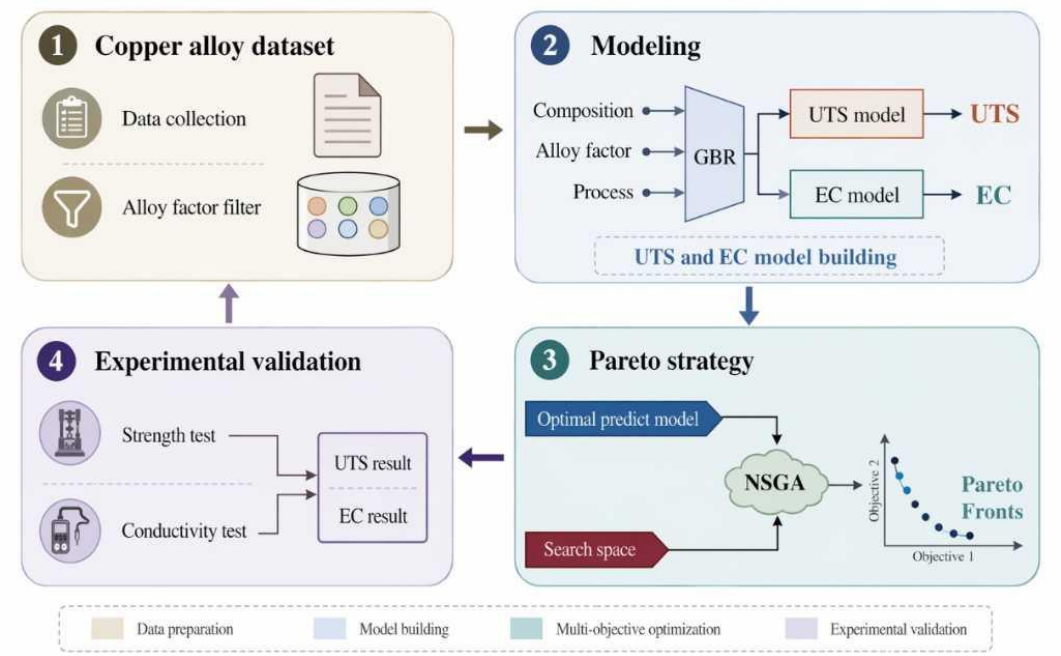

Figure1. Flowchart of the overall design.

Experimental methods

(1) Material preparation

The alloys designed in this work were fabricated via vacuum induction melting under argon protection. High-purity raw materials, including electrolytic copper (99.999 wt%), Ni (99.99 wt%), Co (99.99 wt%), Si (99.99 wt%), Mg (99.95 wt%), and Ag (99.99 wt%), were formulated and melted according to the designed chemical compositions. The dimensions of the obtained ingots were approximately 30 mm *30 mm *50 mm. The detailed thermomechanical processing route is presented in the Supplementary Materials [Supplementary Figure 2]. Furthermore, the actual chemical composition of the optimal alloy was confirmed by inductively coupled plasma optical emission spectrometry (ICP-OES), and the corresponding data are listed in the Supplementary Materials [Supplementary Table 8].

(2) Property test and microscopic observation

In the present work, the mechanical performance of the alloys was assessed with a CMT5205 universal testing machine at a constant tensile rate of 2 mm/min. To ensure data reliability, each specimen was tested three times independently, and the average value was calculated. A strain gauge was used to accurately measure the plastic strain during the testing process. Electrical conductivity (EC) was determined by measuring resistance using a ZY9987 digital micro-ohmmeter at a constant temperature of 25 °C. Triplicate measurements were performed for each sample, and the results were averaged. Microstructural characterization: Scanning electron microscopy (SEM) samples were prepared using electropolishing; electron backscatter diffraction (EBSD) samples were prepared using argon ion milling; transmission electron microscopy (TEM) samples were prepared by ion beam thinning; the angular range for X-ray diffraction (XRD) testing was 30°~95°.

RESULTS

Machine learning results

During the machine learning phase, based on prior research methodologies, the system incorporated seven key alloy descriptors, including atomic radius difference and variance of second ionisation energy. Through exhaustive screening using Random Forests and multi-algorithm comparison[24,26-31], combined with cross-validation to optimise hyperparameters (see the appendix for detailed results), an optimal predictive model for UTS and EC was ultimately developed.

For the UTS and EC models, the optimal combinations of alloying factors obtained via exhaustive screening using random forest are shown in Figure 2a and b, respectively. The corresponding combination for the UTS model is (GPa, delta_r, simga2 and W), while that for the EC model is (GPa, delta_r and W). Subsequently, artificial neural networks (ANN)[28] were used to compare the prediction errors of different feature combinations, further identifying the optimal input as “element content + alloying factors + process parameters” (see the attachment for details). Finally, through a comprehensive comparison of the accuracy and robustness of various machine learning algorithms, GBR was selected as the optimal model. The root mean square errors (RMSE) for its UTS and EC predictions are 57.89 MPa and 6.12% IACS, respectively, as shown in Figure 2g and

h.

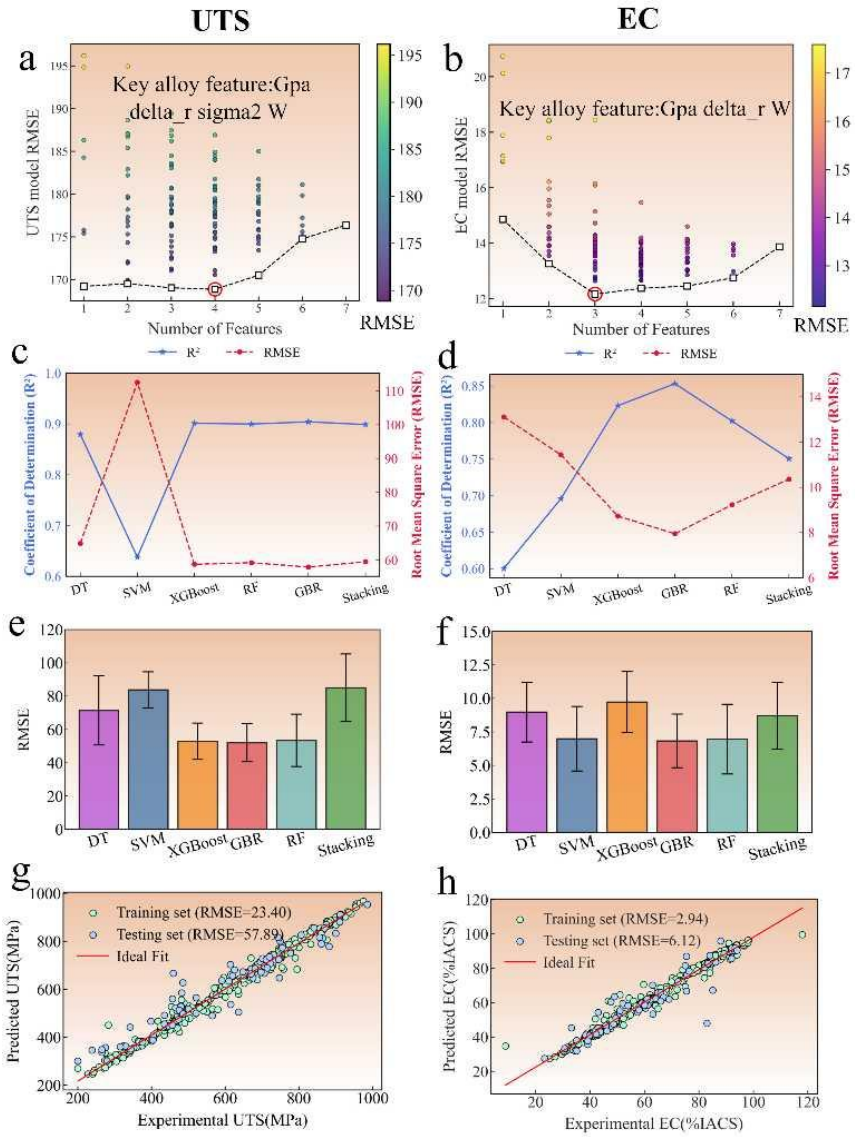

Figure2. Final training results of machine learning models for UTS and EC. ab: results of exhaustive screening of alloy factors using random forest algorithm. cd: comparison of the partitioning effects of training and test sets (2-8 split) for each algorithm; ef: the 10-fold cross-validation results of each algorithm; gh: the optimal prediction models for UTS and EC.

Multi-objective optimisation results

After identifying a UTS and EC gradient-boosted regression model that balances accuracy and robustness, the NSGA-II multi-objective optimization algorithm was used to perform a global search in the six-component space of Ni-Co-Si-Mg-Cr-Ag. The

specific steps are as follows:

(1) Define the search space: Set the mass fraction ranges for elements such as Ni, Co, Si, Mg, Cr, and Ag (in Table 1) and fix the solution treatment, aging, and rolling process parameters (see appendix for details).

(2) Set optimization objectives: Maximize both tensile strength and electrical conductivity.

(3) Perform an NSGA-II search: efficiently identify the set of Pareto-frontier solutions in the composition space, covering three combinations: Cu-Ni-Si-Co-Mg-Cr, Cu-Ni-Si-Co-Mg-Ag, and Cu-Ni-Si-Co-Mg-Ag-Cr;

(4) Output candidate window: Provides a reliable design space for component selection for subsequent experimental validation.

To improve the overall quality of the Pareto solution set, Bayesian hyperparameter optimization was introduced prior to the main NSGA-II search: population size, crossover probability, mutation probability, and the PM distribution index were selected as optimization variables, with the objective of maximizing the hypervolume metric. The process was run for 150 iterations within the search range predefined in the Table 2. Figure 3a, c and e illustrate the Bayesian optimisation process, in which the NSGA-II configuration that generates the maximum hypervolume—i.e., minimises the negative hypervolume—is selected as the optimal one. Figure 3b, d and f present the Pareto front results obtained after 3,000 consecutive generations using the optimised hyperparameters, showing the complete fronts comprising 74, 72 and 100 non-dominated solutions respectively. The TOPSIS method was employed to comprehensively assess the performance ranking of the Pareto front solution set[27], with the specific calculation formula as follows Eq. (1)(2):

$$UTS_{norm}=UTS_i/UTS_{Max} \quad EC_{norm}=EC_i/EC_{Max} \tag{1}$$

$$TOPSIScore = \frac{UTS_{norm}}{UTS_{norm}+EC_{norm}} \quad (2)$$

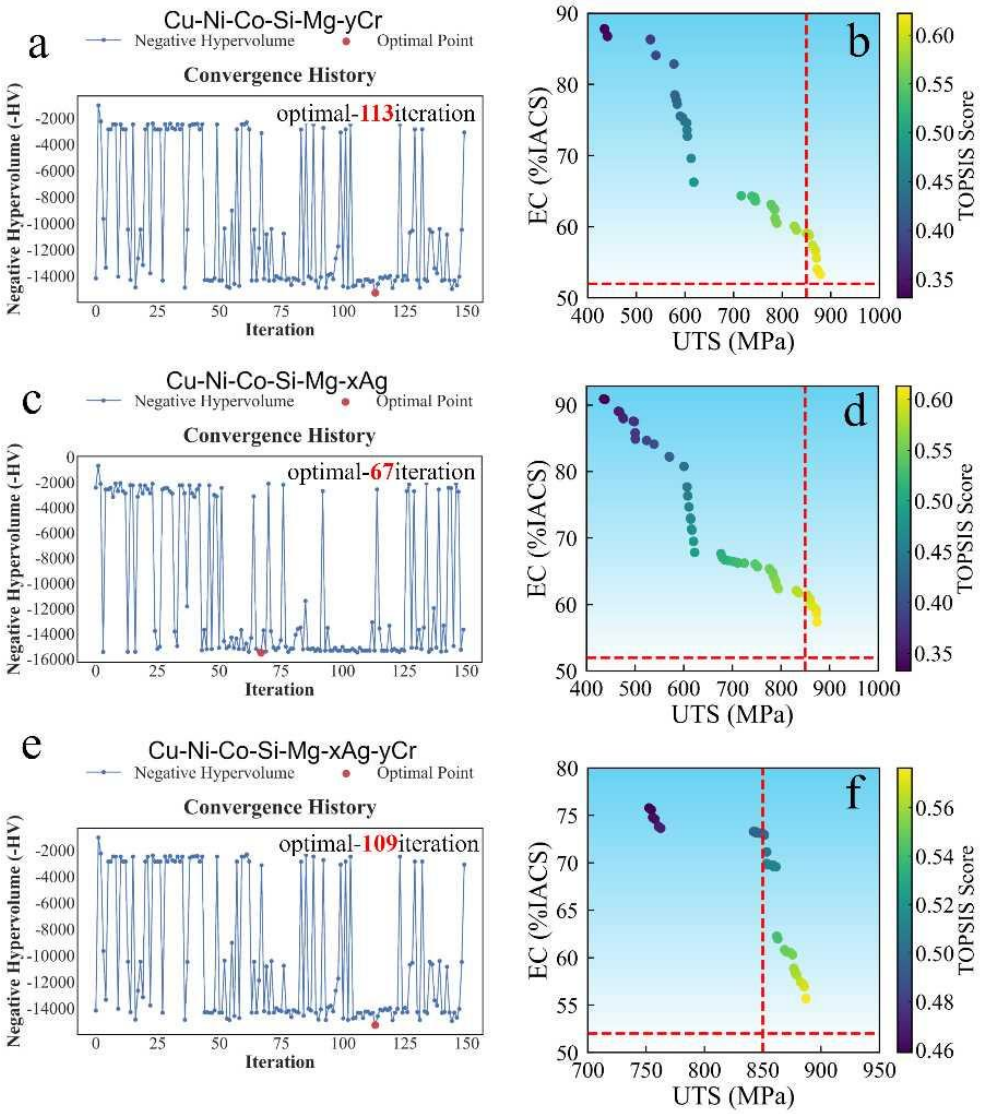

Figure 3. Bayesian iterative parameter process and pareto solution set. ab: Cu-Ni-Co-Si-Mg-Cr space; cd: Cu-Ni-Co-Si-Mg-Ag space; ef: Cu-Ni-Co-Si-Mg-Ag-Cr space.

Table 1. Range of ingredient content(wt%).

Cu	Ni	Co	Si	Mg	Ag	Cr
Bal	0.1~3.0	0.1~2.0	0.1~2.0	0.01~0.5	0~2.0	0
Bal	0.1~3.0	0.1~2.0	0.1~2.0	0.01~0.5	0~2.0	0~2.0
Bal	0.1~3.0	0.1~2.0	0.1~2.0	0.01~0.5	0~2.0	0~2.0

Table 2. NSGA-II algorithm hyperparameters search space.

Pop_size	Crossover_prob	Crossover_eta	Mutation_prob	Mutation_eta
(30,100)	(0.6,0.95)	(5,30)	(0.01,0.3)	(5,30)

Experimental verification result

Given that the strengthening mechanism of Cu-Ni-Co-Si alloys primarily relies on precipitation hardening via the δ-$(Ni,Co)_2Si$ phase[13,14,15,18], and to ensure sufficient formation of the precipitate phase, this study introduced the following constraint across the entire Pareto set: the (Ni+Co)/Si mass ratio is controlled within the range of 4.0~5.4, and the proxy model predictions must satisfy UTS ≥ 850 MPa and EC ≥ 52% IACS. That is, the TOPSIC score for the solution sets corresponding to the space of Cu-Ni-Co-Si-Mg-Cr, Cu-Ni-Co-Si-Mg-Ag, and Cu-Ni-Co-Si-Mg-Ag-Cr should exceed 0.59, 0.59, and 0.49, respectively. After a two-stage screening process, seven representative alloy compositions were ultimately obtained; the detailed results are listed in the Table 3.

Meanwhile, although machine learning enables global optimization of alloy composition to elevate strength as well as electrical conductivity, the rolling and aging treatment exerts a decisive effect on the final properties of age-hardened copper alloys. To attain the maximum combination of high strength and conductivity (target: UTS ≥ 850 MPa, EC ≥ 50 %IACS), multi-step thermomechanical processing was employed in this study for experimental verification based on previous experience (see the appendix for details).

It should be noted that this complex process was not directly applied in the composition design stage for the following reasons: (1) Although multiple rolling-aging cycles can significantly improve properties, the limited availability of existing high-quality data makes reliable modeling difficult; (2) The increase in process parameters will raise the feature dimension and training difficulty, which tends to cause overfitting.

Figure 4a and b show the comparison of predicted versus actual strength and predicted versus actual electrical conductivity for the seven alloys. It is evident that the overall fault rate is low, with 3-alloy (Cu-0.65Ni-1.65Co-0.44Si-0.09Mg-0.46Ag) exhibiting the best overall performance. Figure 4c shows the stress-strain curves of 3-alloy from three independent tensile tests, while Figure 4d evaluates the performance of the designed

copper alloy using the Pareto set method with that of previously reported alloys[32-36]. It is evident that the copper alloy with the best performance designed in this study surpasses the reported copper alloys in terms of the combined strength-conductivity index.

Table 3. Composition of the seven recommended alloys.

id	Si(wt%)	Mg(wt%)	Ni(wt%)	Ag(wt%)	Co(wt%)	Cr(wt%)	(Ni+Co)/Si
1	0.46	0.09	0.65	0	1.72	0.47	5.15
2	0.47	0.14	0.25	0	1.71	0.56	4.17
3	0.44	0.09	0.65	0.46	1.65	0	5.23
4	0.47	0.1	0.65	0.46	1.44	0	4.45
5	0.48	0.14	0.65	0.09	1.72	0.35	4.94
6	0.46	0.14	0.23	0.47	1.97	0.33	4.78
7	0.45	0.14	0.29	0.09	1.72	0.1	4.47

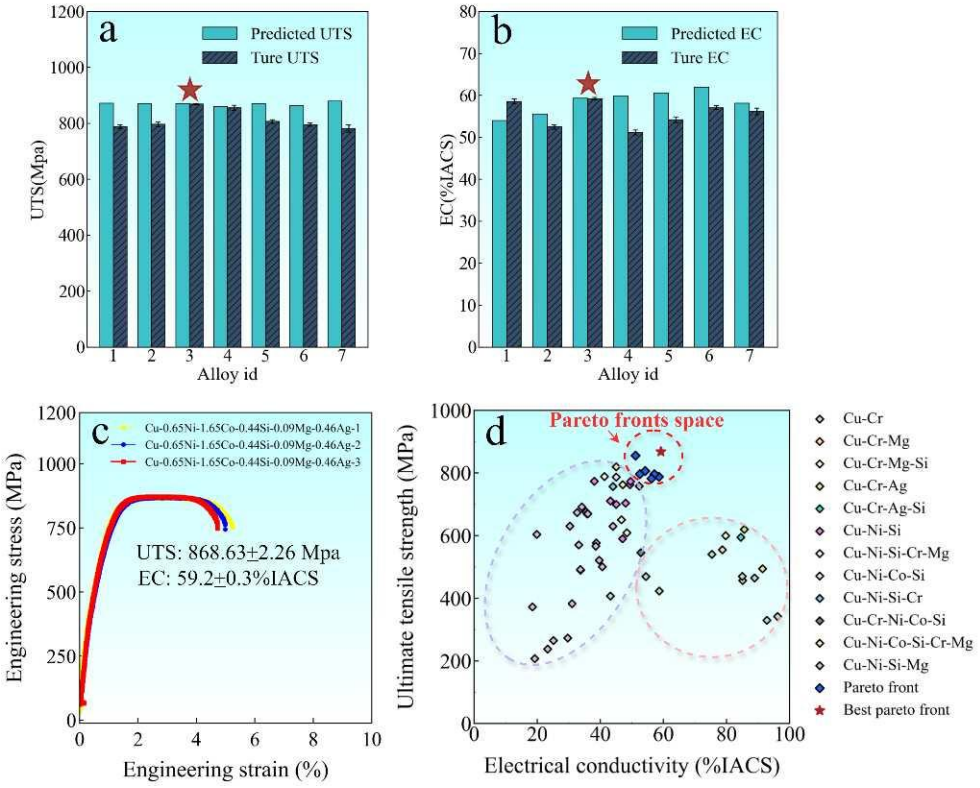

Figure 4. Comparison between predicted and experimental values of the seven alloys, as well as the stress-strain curve of the alloy with optimal performance. (a)(b) Predicted and experimental values of UTS and EC; (c)Cu-0.65Ni-1.65Co-0.44Si-0.09Mg-0.46Ag alloy

stress-strain curve; (d) Performance comparison between the alloys designed in this work and previously reported alloys.

Microstructural characterization

In this section, representative alloys with the highest strength were selected from three alloy systems (Cr-only, Ag-only, and Ag-Cr co-alloyed), namely 2-alloy, 3-alloy, and 5-alloy. Multi-scale characterizations including SEM, EBSD, XRD, and TEM were systematically performed to reveal the impact of alloying elements on the morphology, distribution of precipitates, and the corresponding strengthening mechanisms.

In the Figure5 a, b, and c match to the SEM morphologies and EDS analysis results of alloy 2, 3, and 5, respectively. All three alloys exhibit disc-shaped and rod-shaped precipitates; additionally, coffee bean-shaped precipitates are visible in 2- alloy and 5-alloy[13,14,17,18]. Preliminary EDS analysis of the SEM images in the appendix indicates that the disc-shaped and rod-shaped precipitates are enriched in Ni, Co, and Si; while the bean-like precipitates are enriched in Cr. Further statistical size measurement distribution and area fraction of the precipitates in the three alloys revealed that 3-alloy (Cu-0.65Ni-1.65Co-0.44Si-0.09Mg-0.46Ag) had the smallest average size of fine precipitates (31.35 nm) and the largest area fraction (15.01%).

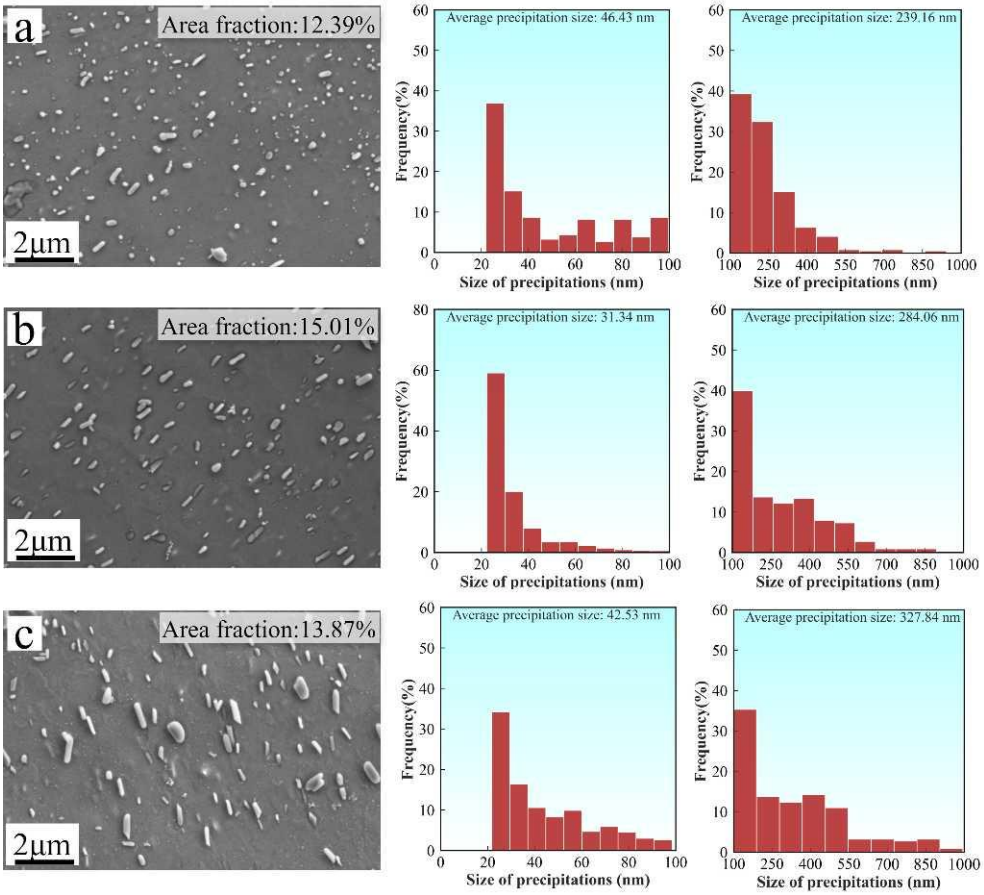

Figure 5. SEM images and size distribution charts of the precipitates from alloys 2, 3, and 5 at the end of the aging period: a.2-alloy(Cu-0.25Ni-1.71Co-0.47Si-0.14Mg-0.56Cr); b.3-alloy(Cu-0.65Ni-1.65Co-0.44Si-0.09Mg-0.46Ag;c.5-alloy(Cu-0.65Ni-1.72Co 0.48Si-0.14Mg-0.35Cr-0.09Ag).

Figure 6 presents the EBSD-IPF orientation maps of alloys 2, 3 and 5. It can be seen that the grains are significantly stretched and fragmented following the rolling direction. Among them, the average grain sizes of 3-alloy and 5-alloy are relatively small, measuring 0.64 μm and 0.65 μm respectively, while the grain size of 2-alloy is relatively large at 0.70 μm.

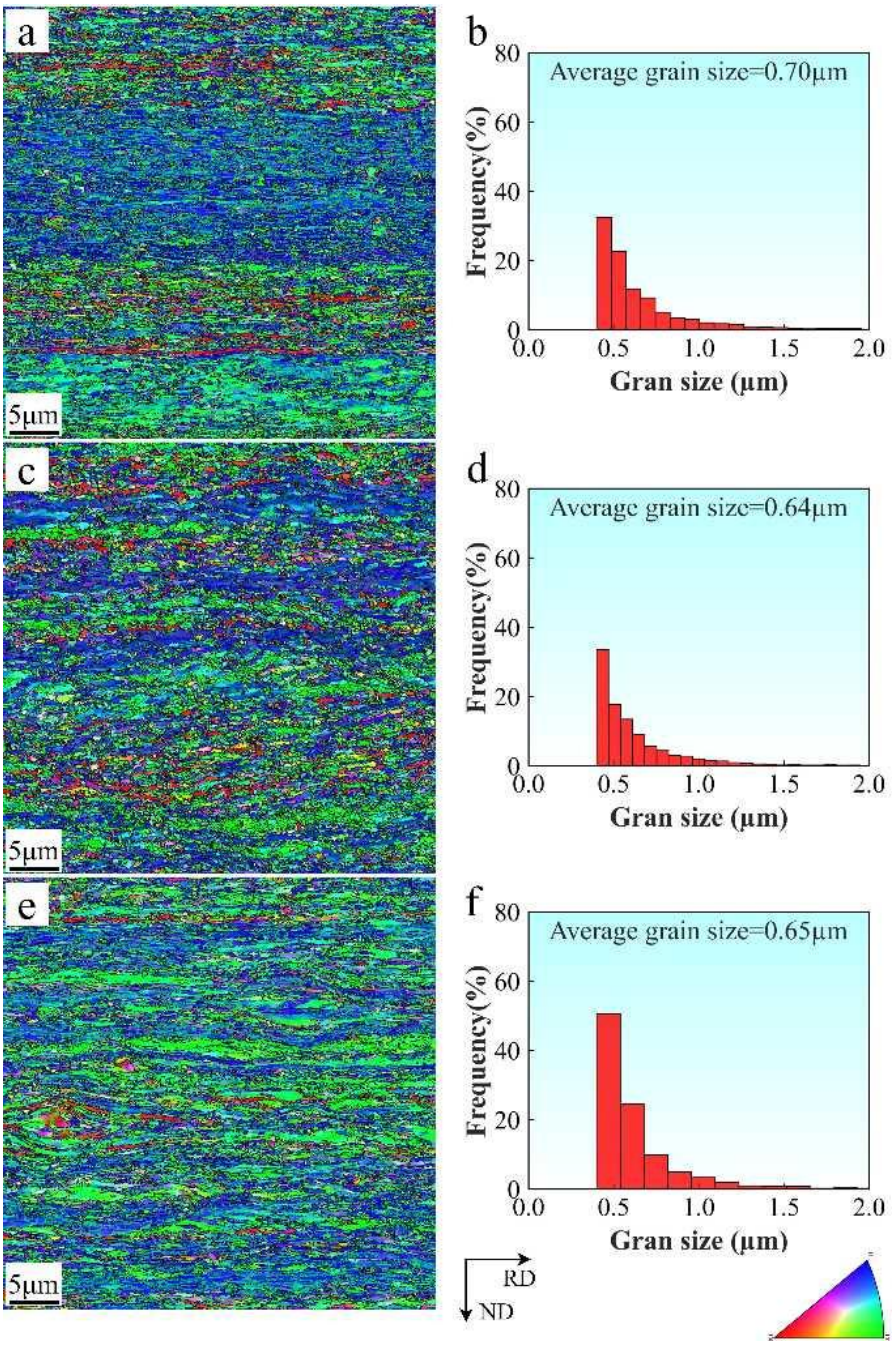

Figure 6. IPF and grain size diagrams of alloys 2, 3, and 5 after final aging. a.2-alloy(Cu-0.25Ni-1.71Co-0.47Si-0.14Mg-0.56Cr); b.3-alloy(Cu-0.65Ni-1.65Co-0.44Si-0.09Mg-0.46Ag; c.5-alloy(Cu-0.65Ni-1.72Co-0.48Si-0.14Mg-0.35Cr-0.09Ag).

Figure 7 shows the XRD diffraction patterns of alloys 2, 3 and 5. The average dislocation densities of the three alloys were estimated via XRD phase identification and micro-stress calculation, so as to compare the contribution of dislocation strengthening. Lattice

distortion results in the broadening of diffraction peaks; the average micro-strain of the alloys can be estimated by analyzing the variation of peak broadening with diffraction angle, and the micro-strain is closely related to dislocation density, as shown in Eq (3)(4). According to relevant literature[11], four strong diffraction peaks in the range of 30~95° were identified to correlate with the Cu-(111), Cu-(200), Cu-(220), and Cu-(311) crystal planes, respectively. The microstrain and dislocation density of the three alloys were obtained by fitting and analyzing the XRD diffraction peaks using Jade 6 software. The dislocation densities were determined to be $4.66 \times 10^{14}m^{-2}$, $5.88 \times 10^{14}m^{-2}$ and $5.39 \times 10^{14}m^{-2}$ respectively. The results demonstrate that 3-alloy possesses the highest dislocation density, indicating its most pronounced dislocation strengthening effect.

$$\varepsilon=\frac{\beta^{*}cos\theta}{4sin\theta} \quad (3)$$

$$\rho=\frac{2\sqrt{3}\varepsilon}{d_G b} \quad (4)$$

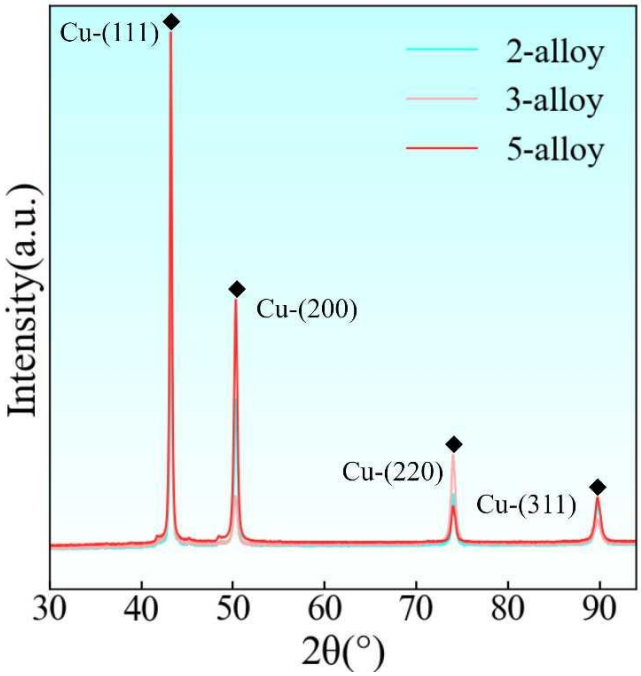

Figure 7. XRD patterns of alloys 2, 3, and 5 after final aging. 2-alloy: Cu-0.25Ni-1.71Co-0.47Si-0.14Mg-0.56Cr; 3-alloy:Cu-0.65Ni-1.65Co-0.44Si-0.09Mg-046Ag; 5-alloy:Cu-0.65Ni-1.72Co-0.48Si-0.14Mg-0.35Cr-0.09Ag.

The Figure 8 shows the TEM morphologies of alloys 2, 3, and 5, along with the matching SAED patterns; the specific regions are marked as “Area” in the figure. For 2-alloy, the relative orientation between the disc-shaped precipitates and the copper matrix is as follows:$[\bar{1},\bar{1},0]_{Cu}//[\bar{1},0,0]_{\delta},(1,\bar{1},0)_{Cu}//(0,\bar{1},\bar{2})_{\delta}$; For Alloy 3, the orientation relationship between the rod-shaped precipitates and the matrix is determined:$[\bar{1},\bar{1},0]_{Cu}//[1,0,0]_{\delta},(1,\bar{1},\bar{1})_{Cu}//(0,1,\bar{2})_{\delta}$; In 5-Alloy t the orientation relation between the rod-shaped precipitates and the matrix is $[0,\bar{1},\bar{1}]_{Cu}//[\bar{3},\bar{2},1]_{\delta},(1,\bar{1},\bar{1})_{Cu}//(0,1,\bar{2})_{\delta}$. Along with the EDS analytical results from SEM, the precipitates are identified as mainly the δ-$(Ni,Co)_2Si$ phase[17,18].

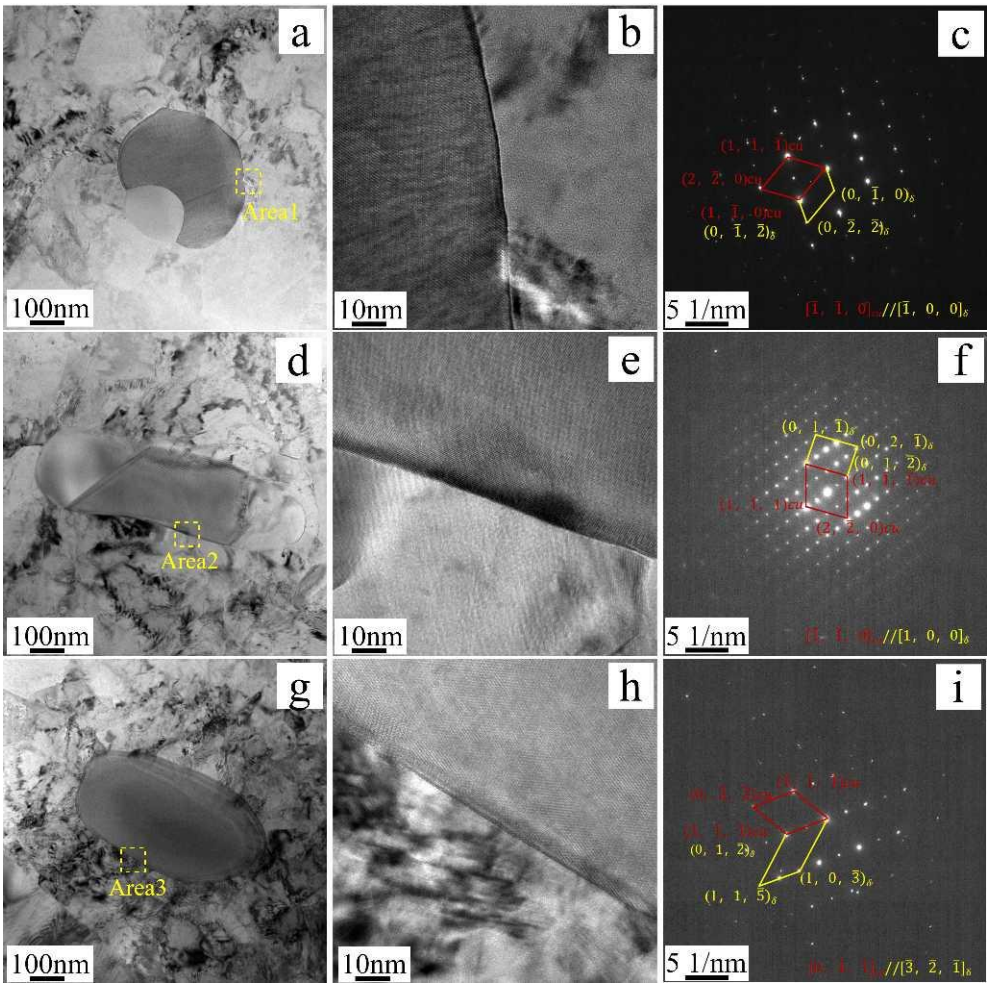

Figure 8. Bright-field, HRTEM and SAED images of alloys 2, 3, and 5 after final aging. abc: 2-alloy (Cu-0.25Ni-1.71Co-0.47Si-0.14Mg-0.56Cr); def:3-alloy(Cu-0.65Ni-

1.65Co-0.44Si-0.09Mg-046Ag); ghi:5-alloy(Cu-0.65Ni-1.72Co-0.48Si-0.14Mg-0.35Cr-0.09Ag).

Figure 9 shows the TEM morphologies, dislocation and precipitate distributions, and statistical results of the precipitate sizes for alloys 2, 3, and 5. TEM observations of 3 alloy reveal extensive dislocation entanglement, its dislocation density is significantly higher than those of 2-alloy and 5-alloy which supports the trend of dislocation densities obtained by XRD fitting. Figure10 EDS surface scanning further indicates a high-density, uniformly dispersed distribution of nanoscale δ-$(Ni,Co)_2Si$ particles in the 3-alloy. In Figure 9f, quantitative statistical analysis shows that 3-alloy has the smallest average precipitate size (10.62 nm) and the highest volume fraction (3.19%). The synergistic effect of high-density dislocation entanglement and fine, uniformly distributed precipitates enhances both dislocation strengthening and precipitation strengthening, thereby further contributing to the yield strength and significantly improving the strength of 3-alloy. The physical parameters obtained through systematic characterization including dislocation density, precipitation phase characteristics, and grain size are summarized in Table 4.

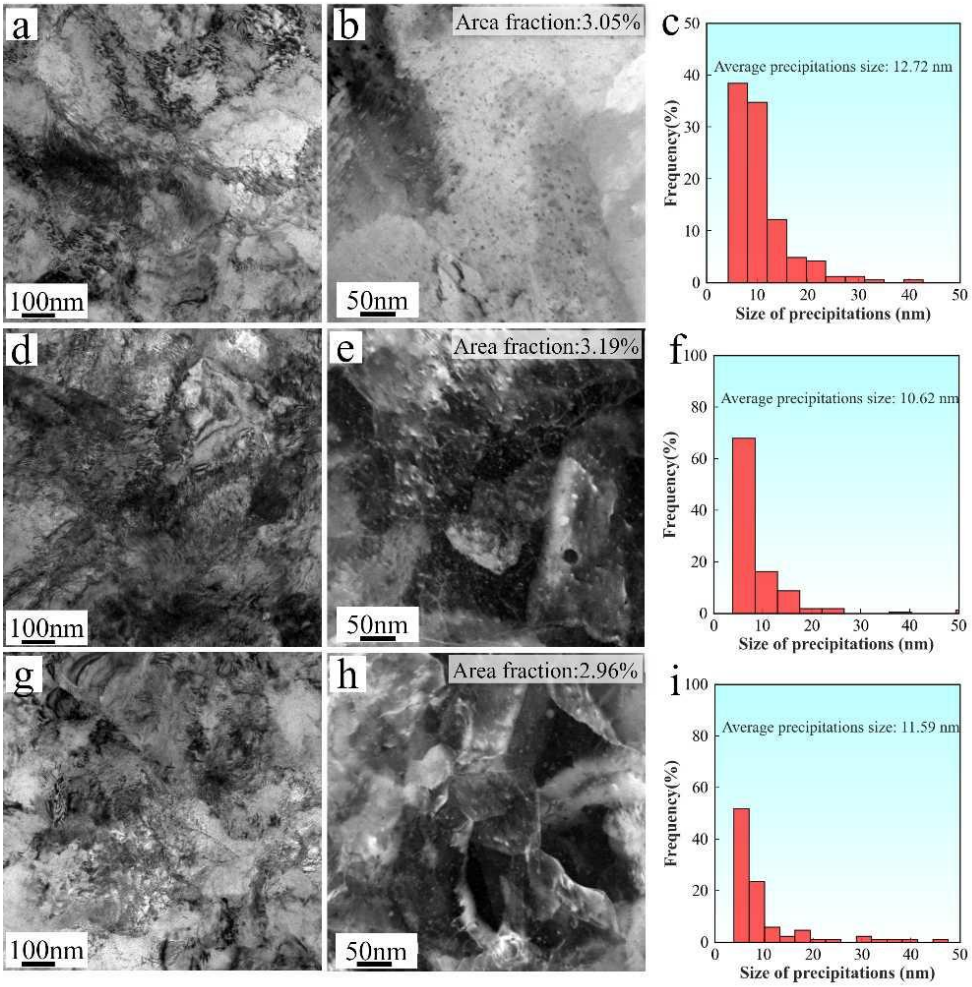

Figure 9. TEM images showing dislocation and precipitate distributions of alloys 2, 3, and 5 after final aging, along with precipitate size distribution charts. abc: 2-alloy (Cu-0.25Ni-1.71Co-0.47Si-0.14Mg-0.56Cr); def: 3-alloy (Cu-0.65Ni-1.65Co-0.44Si-0.09Mg-046Ag); ghi: 5-alloy (Cu-0.65Ni-1.72Co-0.48Si-0.14Mg-0.35Cr-0.09Ag).

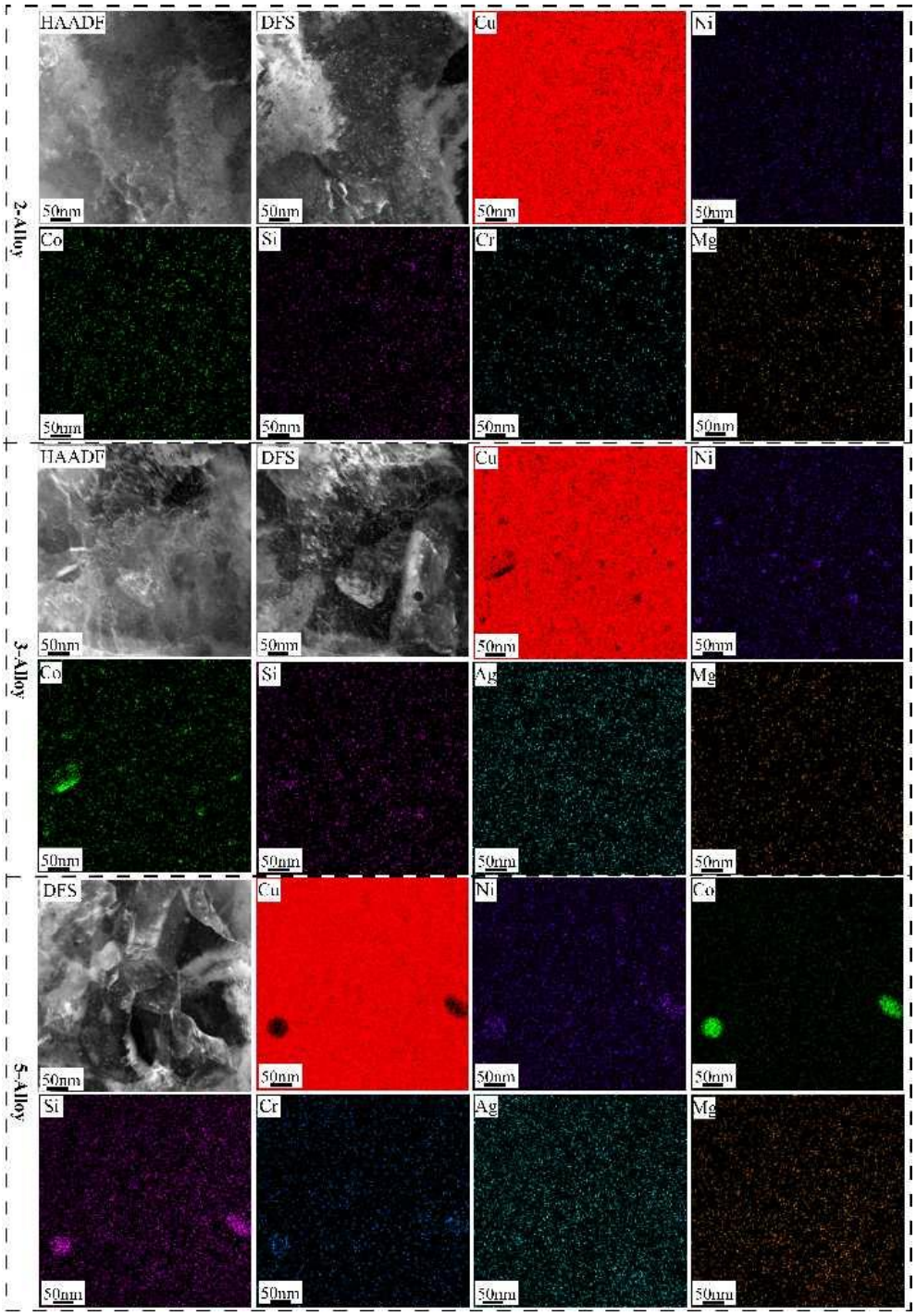

Figure 10. HADDF and dark field images of alloys 2, 3, and 5 after final aging, as well as EDS analysis results of each element. 2-alloy: Cu-0.25Ni-1.71Co-0.47Si-0.14Mg-0.56Cr;3-alloy: Cu-0.65Ni-1.65Co-0.44Si-0.09Mg-046Ag; 5-alloy: Cu-0.65Ni-1.72Co-0.48Si-0.14Mg-0.35Cr-0.09Ag.

Table 4. For alloys 2, 3, and 5 after final aging: strain(ε), dislocation density(ρ), average precipitate size(d_p) and volume fraction(f_v), and grain size(d).

Alloy-Id	Dislocation		Precipitation		Grain
	ε(%)	$\rho(10^{14}/m^2)$	d_p(Nm)	f_v(%)	d(μm)
2	0.240	4.65	12.72	3.05	0.70
3	0.277	5.88	10.62	3.19	0.64
5	0.258	5.40	11.59	2.96	0.65

DISSCUSSION

Rational analysis of key factors

Through SHAP interpretability[37] analysis of models for ultimate tensile strength (UTS) and electrical conductivity (EC), this study elucidated the physical mechanisms underlying the influence of optimal alloying elements on material performance, as shown in the Figure 11. In Cu-Ni-Co-Si alloys, the increase in UTS is primarily credited to the effect of nanoscale $(Ni, Co)_2Si$ precipitation phases formed during the aging process. SHAP results indicate that the variance in sigma2 carries the highest weight and exhibits a positive correlation. This reflects subtle differences in the electronic structure between Ni, Co, and Cu; when dislocation lines attempt to cut through or bypass the precipitates, they must overcome an additional energy barrier caused by chemical bonding heterogeneity, which is one of the reasons why the strength of this alloy system exceeds that of the Cu-Ni-Si system. The high positive association between GPa and UTS validates the contribution of the precipitates as hard intermetallic compounds. The higher-order terms of the W capture the strong covalent bonding within the precipitate phase, influencing its ability to pin dislocations during deformatio. The delta_r also manifests as a positive gain in the UTS model. For one thing, the distortion caused by solute atoms provides the basis for solute strengthening; by contrast, delta_r determines the congruent strain field between the precipitate phase and the matrix.

In stark contrast to the UTS model, the EC model is dominated by the compressibility of the delta_r and exhibits a very strong negative correlation. Electrical conductivity depends on the mean free path of electrons. In the Cu-Ni-Co-Si system, the delta_r between Ni, Co, and Si atoms and Cu is the primary source of scattering. SHAP results clearly reveal the importance of the matrix purification effect: the purity of the matrix is restored only when the aging process causes these size-mismatched solute atoms to fully

incorporate into the $(Ni,Co)_2Si$ precipitation phase. The Gpa and W have a relatively minor negative impact on EC; during the precipitation-hardening-dominated stage, these effects are typically masked by distortion scattering caused by residual solutes.

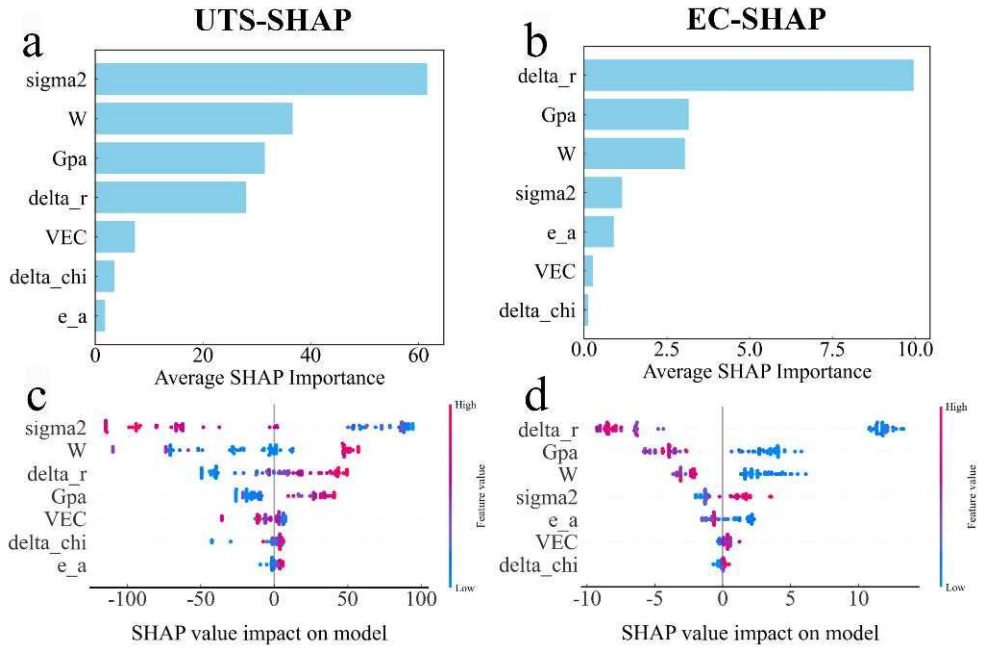

Figure 11. SHAP analysis results of each alloy factor. ab: alloy factor SHAP importance distribution chart; cd: alloy factor contribution chart.

Reliability analysis of the pareto set

To validate the reliability of the Pareto solution set, this study conducted relevance analysis and quadratic fitting on the solution set of Cu-Ni-Co-Si-Mg-Ag alloy composition combinations, with results presented in the Figure 12. Scatter plot analysis of Ni, Co, Si, Mg, and Ag content versus UTS and EC properties within the solution sets reveals that all solutions adhere to metallurgical principles: increased alloying element content enhances strength whilst decreasing electrical conductivity. This occurs because alloying elements strengthen the alloy through solid solution distortion and secondary phase precipitation, yet simultaneously reduce conductivity due to lattice distortion and electron scattering. The recommended element combinations been randomly generated, it would be impossible for all solutions to conform to metallurgical principles. This validates the rationality and reliability of the Pareto solutions.

Furthermore, the analysis revealed the influence patterns of primary alloying elements

(Ni, Co, Si) on alloy properties, which fully aligns with the precipitation strengthening mechanism of Cu-Ni-Co-Si-based alloys. Specifically, the formation of the $(Ni,Co)_2Si$ phase is directly regulated by the ratio of Ni, Co, and Si content. For Co and Ni elements, their correlations with alloy strength reached 0.93 and 0.7 respectively, while their correlations with electrical conductivity were -0.91 and -0.61 respectively. This indicates that Co exerts the most significant influence on properties among all elements. Notably, Co exhibits higher solubility in copper than Ni, meaning Co can sustainably contribute to precipitation strengthening across a broader composition range. Furthermore, prior research indicates that minor Co additions significantly diminish the interfacial energy between the copper matrix and precipitates, with low interfacial energy accelerating the generation of the $(Ni,Co)_2Si$ precipitation phase.

Compared to primary alloying elements, trace alloying elements such as Mg and Ag exhibit a complex trend in their influence on properties, characterised by initial increases followed by decreases, or initial decreases followed by increases. Notably, the alloy strength only shows a significant improvement when the addition levels of Mg and Ag reach a certain threshold. Among these trace alloying elements, the addition of Ag exerts the most negligible effect on electrical conductivity. Consequently, the data indicates that Ag is an excellent trace alloying element capable of enhancing strength while minimising conductivity loss. Indeed, this conclusion is supported by existing experimental evidence. In summary, through correlation analysis, quadratic fitting, and in-depth examination of elemental characteristics, it is concluded that the Pareto solution set is both effective and reliable, accurately reflecting the regulatory relationship between composition and properties.

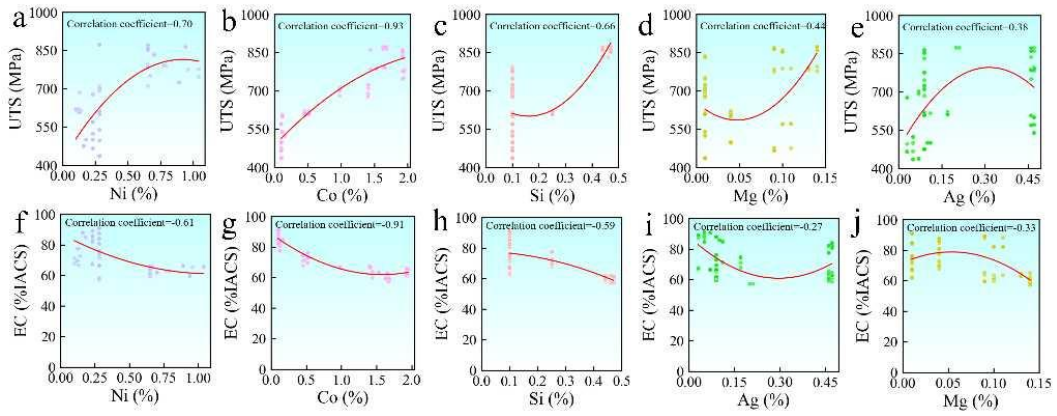

Figure 12. Distribution of elements content and properties in the pareto set. abcde: distribution of the effects of Ni,Co,Si,Mg,Ag content and UTS; fghij: distribution of the effects of Ni,Co,Si,Mg,Ag content and EC.

Strengthening mechanism and conductive mechanism

(1) Strengthening mechanism

The increase in yield strength of the copper alloy optimized using the NSGA-II algorithm stems from the synergistic interaction of multiple strengthening mechanisms, as expressed in the following Eq (5). Here, σ_0 represents the peierls stress of copper, which is 52 MPa[47], while σ_s, σ_g,σ_p and σ_d denote the sources to the yield strength from solution strengthening, grain boundary strengthening, precipitation strengthening, and dislocation strengthening, respectively[40].

$$\sigma_{alloy}=\sigma_0+\sigma_s+\sigma_d+\sigma_p+\sigma_g \quad (5)$$

the factors contributing of solid solution strengthening to the yield strength can be calculated using the following Eq (6)(7)[41]. For Cu-Ni-Co alloys, this calculation is based on the following simplifying assumption: Co and Si exist as secondary precipitates; therefore, only the contributions of Cr, Ni, Ag and Mg to solid solution strengthening are considered. The parameters in the equation are defined as follows: r_s is the radius of the solute atom, r_m is the radius of the Cu atom, x_a is the molar fraction of the solute atom, δ is the lattice variation factor, and G is the shear modulus of copper, which is 45.5 GPa[42].

$$\delta=\frac{|r_s-r_m|}{r_m} \quad (6)$$

$$\sigma_s=\sum G\,\delta x_a^{\frac{3}{2}}\sqrt{\frac{x_a}{3}} \quad (7)$$

The Hall-Petch calculation expression for grain boundary strengthening[42]is given by Eq (8). K is a constant equal to 0.18 Mpa·m$^{1/2}$, and d is the average grain diameter.

$$\sigma_g=Kd^{-1/2} \quad (8)$$

The contribution of precipitation hardening to the yield strength can be calculated using the following Eq (9)(10)[37]: In the equation, b is the Burgers vector (0.255 nm), v is the poisson's ratio (0.34), M is the Taylor factor (3.1 for copper alloys), λ is the effective interparticle spacing accounting for the size effect of the barrier, and d_p and f_v are the average diameter and volume fraction of the precipitates, respectively; f_v is approximated by measuring the area fraction in transmission electron microscope images using Image-Pro Plus software.

$$\lambda=\frac{1}{2}d_p*\sqrt{\frac{3\pi}{2f_v}} \tag{9}$$

$$\sigma_p=\frac{0.81MGb\,ln\left(\frac{d_p}{b}\right)}{2\pi(1\text{-}v)^{1/2}(\lambda\text{-}d_p)} \tag{10}$$

The yield strength attributable to dislocation strengthening can be calculated using the following Eq (11)[37], where α is a constant equal to 0.2 and ρ is the dislocation density.

$$\sigma_d=MG\alpha b\sqrt{\rho} \tag{11}$$

The theoretical yield strengths of the three samples designed using the pareto strategy were calculated using Eq (5). Table 5 lists the yield strength increments from each strengthening mechanism and compares the differences between the theoretical calculations and the experimentally measured values. As shown in Figure 13, the strength improvement in the three alloy specimens primarily stems from precipitation hardening and grain boundary hardening, while the contributions from dislocation hardening and solid solution hardening are relatively weaker.

Table 5. Calculation of theoretical yield strength for alloys.

Id	σ_o (Mpa)	σ_g (Mpa)	σ_s (Mpa)	σ_p (Mpa)	σ_d (Mpa)	$\sigma_{calculate}$ (Mpa)	σ_{exp} (Mpa)	error (%)

2	52	215.4	2.05	332.05	153.24	754.74	731.21	+3.21
3	52	225	2.3	389.66	172.18	841.11	854.67	-1.55
5	52	223.26	2.3	357.14	164.89	799.59	780.83	-2.40

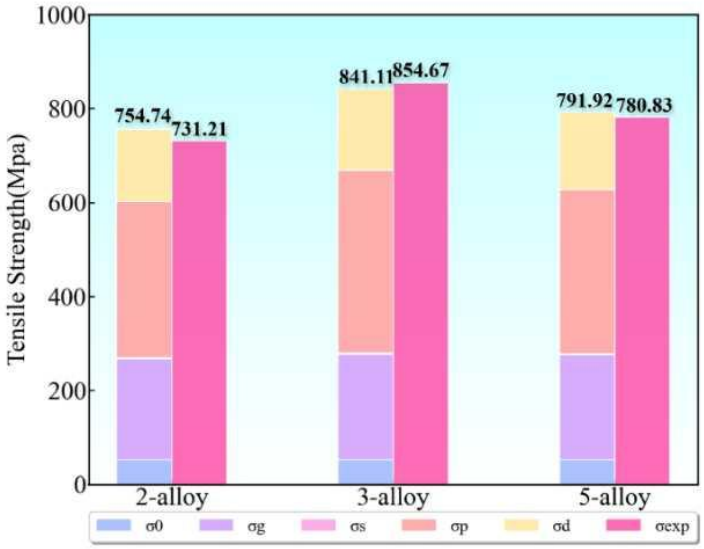

Figure 13. Comparison of experimental and calculated tensile strength.

(2) Mechanism of electrical conductivity

Using the International Annealed Copper Standard (IACS) as a reference, the resistivity of other alloys is calculated using Eq (12)[10]. In this equation, ψ represents the conductivity in %IACS, and ρ_{alloy} represents the resistivity of the alloy.

$$\rho_{alloy}=\frac{1.7241*10^{-10}}{\psi} \quad (12)$$

According to Massison's law[44], the resistivity of an alloy is influenced by microstructural features such as grain boundaries, dislocations, and precipitates; its total resistivity can be calculated using the following Eq (13). In the equation, ρ_0, ρ_G, ρ_d, ρ_{ss} and ρ_p represent the contributions to the resistivity of pure copper (1.72×10^{-8} Ω·m)[48], grain boundaries, dislocations, solute atoms, and precipitates, respectively. Given that the average spacing of the precipitated phases in the three alloys designed by this institute is greater than the mean free path of electrons in pure copper (42 nm)[10], the effect of the precipitated phases

on electrical conductivity can be neglected.

$$\rho_{alloy}=\rho_0+\rho_G+\rho_d+\rho_{ss}+\rho_p \quad (13)$$

Eq (14) given describes the change in resistivity caused by dislocations. Here, A_d is a constant of $2.7 \times 10^{-25}\Omega \cdot m^3$[39], and ρ is the dislocation density of the copper alloy.

$$\rho_d=\rho^* A_d \quad (14)$$

The increase in resistivity caused by electron scattering at grain boundaries can be described by the following Eq (15)[46]. Here, A_G is the constant 3.58×10^{-16}, and d_G is the average grain size.

$$\rho_G=\frac{A_G}{d_G} \quad (15)$$

In this study, the contribution of solute atoms to the resistivity ρ_{ss} was determined by subtracting the dislocation contributions ρ_G grain boundaries ρ_d and the pure copper matrix ρ_0 from the overall resistivity of the alloy. The effects of each factor on the alloy's resistivity and conductivity $\Delta\psi$ are shown in Table 6. The results indicate that solute atoms have the greatest adverse effect on the alloy's electrical conductivity.

Table 6. The increments in resistivity and their respective contributions to the decrease in conductivity.

Id	ρ_{alloy} ($10^{-8}\Omega$.m)	$\Delta\rho_d$ ($10^{-11}\Omega$.m)	$\Delta\rho_G$ ($10^{-10}\Omega$.m)	$\Delta\rho_s$ ($10^{-8}\Omega$.m)	$\Delta\psi_d$ (%IACS)	$\Delta\psi_G$ (%IACS)	$\Delta\psi_s$ (%IACS)
2	3.28	1.26	8.9	3.18	-0.18	-1.29	-46.02
3	2.91	1.59	9.68	2.8	-0.22	-1.36	-39.22
5	3.18	1.46	9.18	3.07	-0.21	-1.32	-44.25

Changes in composition and property

Ni, Co, and Si are the core elements in the Cu-Ni-Co-Si precipitation-hardening alloy system, with their content and ratio directly determining the volume fraction, size distribution, and strengthening efficiency of the precipitation phase. To quantitatively elucidate the influence of these factors on strength and electrical conductivity, this study systematically analyzed seven experimental alloys systems to investigate the relationship between Ni+Co+Si content, the (Ni+Co)/Si mass ratio, and tensile strength and electrical conductivity. The results are presented in the Figure14.

As shown in Figure14d, within the same category of alloying elements, the tensile strength of the alloy exhibits an overall upward trend with increasing total content of Ni, Co, and Si. This is because a rise in the overall content of Ni, Co, and Si is typically coupled with an increase in the number of precipitates that can be formed, and the fractional volume of these precipitates is one of the key factors influencing the mechanical properties of the alloy. The increased number of precipitates enhances the strengthening effect of the precipitated phases, thereby increasing the alloy's tensile strength. Consequently, the trend in tensile strength closely parallels the variation in the total content of Ni + Co + Si.

As shown in Figure 14. a and b, overall, electrical conductivity tends to decrease with increasing total content of Ni, Co, and Si. However, when the (Ni+Co)/Si mass ratio reaches approximately 5.2, the alloy maintains relatively high conductivity even with a total Ni+Co+Si content of around 2.7 wt%. The electrical conductivity of the alloy is primarily influenced by the alloying elements dissolved in the matrix. When the (Ni+Co)/Si mass ratio is excessively low, excessive Si dissolves into the copper matrix, leading to increased lattice distortion and significantly enhanced electron scattering, thereby markedly reducing conductivity. As the (Ni+Co)/Si ratio increases to approximately 5.2, Ni and Co can form nearly complete precipitation phases with Si, significantly reducing the residual solute in the matrix and thereby maximising electrical

conductivity.

The Cu-0.65Ni-1.65Co-0.44Si-0.09Mg-0.46Ag alloy, engineered through machine learning and multi-objective optimisation, exhibits a total Ni+Co+Si content of 2.74 wt% and a (Ni+Co)/Si ratio of 5.23. The alloy's exceptional properties stem primarily from the precise ratio of Ni, Co and Si, coupled with the synergistic effects of Mg and Ag. Notably, the addition of Ag further enhances both the alloy's strength and electrical conductivity. Machine learning and multi-objective optimisation techniques played a pivotal role in recommending the composition. In this study, by setting the (Ni+Co)/Si ratio range within the potential pareto solution set at 4.0~5.4 wt% and targeting a tensile strength of 850 MPa and electrical conductivity of 52% IACS, the alloy composition meeting performance requirements was successfully identified after only seven experimental verifications, significantly enhancing design efficiency.

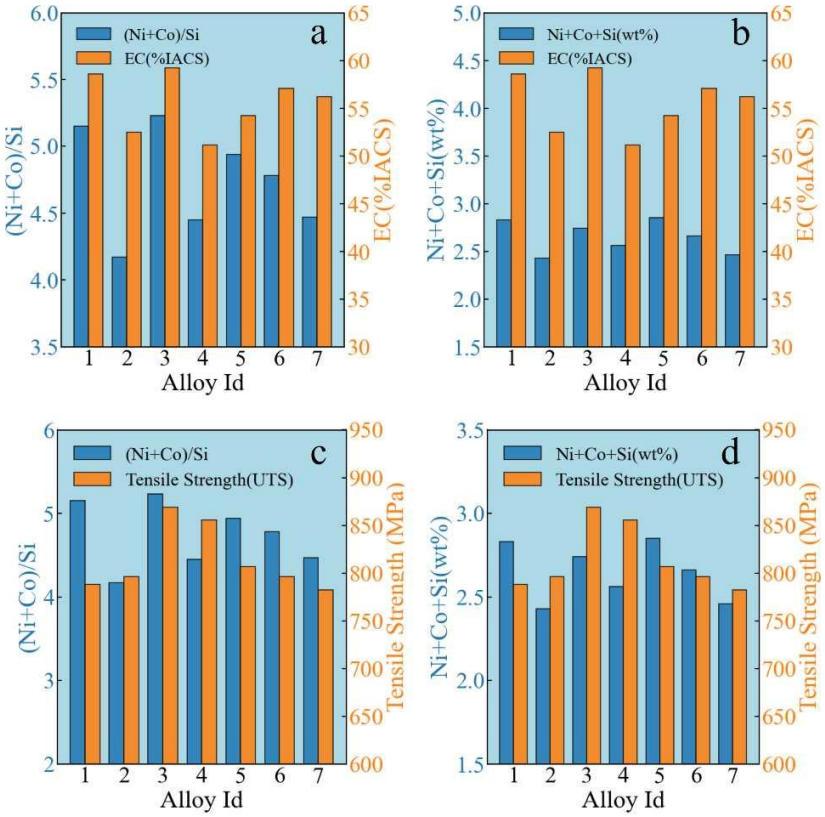

Figure 14. Analysis of the Relationship between Ni, Co and Si content combinations and performance variations.

Most existing studies have mainly focused on preparing high-strength Cu-Ni-Si alloys by adding elements such as Co, Mg, Cr, Ti. For example, Zhang *et al.*[13] designed a Cu-1.3Ni-1.4Co-0.56Si-0.03Mg alloy via machine learning, achieving a tensile strength of 858 MPa and an electrical conductivity of 47.6 %IACS. Guo *et al.*[46] developed a Cu-3Ti-0.3Cr-0.15Mg alloy with an ultrahigh tensile strength of 1,018 MPa, but its electrical conductivity was only 20.1 %IACS. However, the electrical conductivity of these alloys is generally below 50% IACS. In this study, machine learning and the NSGA-II multi-objective optimization algorithm were used to rapidly design alloy compositions. It was found that the addition of trace Ag can synergistically optimize the Cu-Ni-Si alloy system, enabling a considerable improvement in electrical conductivity while maintaining high strength. This finding provides a new compositional design strategy and material selection scheme for copper alloys with high strength and electrical conductivity for integrated circuit lead frames.

CONCLUSION

This study successfully achieved the rapid design of novel high-strength, high-conductivity copper alloy compositions by combining machine learning with the NSGA-II algorithm. The main conclusions are as follows:

(1) By incorporating key alloy parameters such as sigma2 and delta_r, optimal prediction models for UTS and EC were developed, with RMSE values of 57.89 MPa and 6.12% IACS, respectively. Subsequently, by integrating Bayesian hyperparameter optimization with the NSGA- II Pareto set strategy, efficient optimization was carried out in the six-dimensional composition space. Combined with prior process development experience, the multi-pass rolling and aging window was fixed, enabling rapid screening of seven candidate compositions for high-strength and high-conductivity copper alloys. Experimental verification shows that the average error rate between measured and predicted properties is less than 8%, confirming the reliability of the “machine learning-

multi-objective optimization-empirical synergy" design paradigm.

(2) Cu-0.65Ni-1.65Co-0.44Si-0.09Mg-0.46Ag alloy with a tensile strength of 868.63 MPa and a conductivity of 59.2 % IACS was successfully designed. Its primary strengthening mechanisms are precipitation hardening and grain refinement; the effects of grain boundaries, dislocations, and precipitates on resistivity are limited, while the solid solution of solute atoms is the main cause of the increase in resistivity.

(3) In the optimized alloy, Ni, Co, and Si interact synergistically with trace amounts of Ag and Mg. The composition is Ni + Co + Si = 2.74 wt%, with a (Ni + Co)/Si ratio of 5.23. The Ag and Mg element significantly promotes the formation of nanoscale precipitation phases, cooperatively improving both the alloy's strength and electrical conductivity.

DECLARATIONS

Authors' contributions

Writing - original draft, Investigation: Li YH;

Writing - review & editing, Investigation: Xu J;

Writing - review & editing, Writing - original draft, Investigation, Formal analysis, Data curation: Guan B;

Formal analysis, Investigation: Wu D;

Formal analysis, Investigation: Han YS, Pan XK, Xu HD, Ma GH;

Formal analysis, Supervision: Hu Z;

Project administration, Formal analysis: Hu Q.

Availability of data and materials

Partial results verifying the conclusions of this study are presented in the Supplementary Materials, and the complete Pareto solution set is displayed in Other File. The remaining

raw data supporting the findings of this study are available from the corresponding author upon reasonable request.

Financial support and sponsorship

This paper acknowledges the supported by Key R&D Projects of Jiangxi Province (20261BCE310067), Jiangxi Key Laboratory of Advanced Copper-based Materials (2024SSY05021).

Conflict of interest

The authors declare that they have no known competing financial interests or personal relationships that could have appeared to influence the work reported in this paper.

Ethical approval and consent to participate

Not applicable.

Consent for publication

Not applicable.

REFERENCES

[1] Yang L, Zhang FY, Yan MF, Zhang ML. Microstructure and mechanical properties of multiphase layer formed during thermo-diffusing of titanium into the surface of C17200 copper-beryllium alloy. *Applied Surface Science,* 2014, 292: 225-30.[DOI: 10.1016/j.apsusc.2013.11.121]

[2] Guoliang X, Qiangsong W, Xujun M, Baiqing X, Lijun P. The precipitation behavior and strengthening of a Cu-2.0wt% Be alloy. *Materials Science & Engineering A,* 2012, 558: 326-30.[DOI: 10.1016/j.msea.2012.08.007]

[3] Song Y, Yang J, Song K, et al. Effect of tensile stress annealing on residual stress and

strength of C19400 alloy. *Journal of Materials Research and Technology,* 2023, 25: 786-98.[DOI: 10.1016/j.jmrt.2023.05.253]

[4] Zhou F, Zhang Y, Lu L, Song K, Gao H. Effects of a thermal-ultrasonic stress relaxation process on the residual stress, mechanical properties and microstructures of C19400 copper alloy strips. *Materials Science & Engineering A,* 2022, 841: 143014.[DOI: 10.1016/j.msea.2022.143014]

[5] Yang J, Bu K, Zhou Y, et al. Influence of short-time annealing on the evolution of the microstructure, mechanical properties and residual stress of the C19400 alloy strips. *Journal of Alloys and Compounds,* 2023, 941: 168705.[DOI: 10.1016/j.jallcom.2023.168705]

[6] Liao W, Yang H, Yi C, Zheng J. Effect and mechanism of cold rolling and aging process on microstructure and properties of columnar grain C70250 copper alloy. *Materials Science & Engineering A,* 2022, 833: 142577.[DOI: 10.1016/j.msea.2021.142577]

[7] Liao W, Qiang H, Song W, Hu Y, Zhang C. Effect and mechanism of room temperature rolling, cryogenic rolling and heat treatment on mechanical properties and electrical conductivity of Cu-Ni-Si alloy with continuous directional solidification. *Journal of Alloys and Compounds,* 2023, 949: 169748.[DOI: 10.1016/j.jallcom.2023.169748]

[8] Liao W, Hu Y, Liu Q. High strength and high electrical conductivity C70250 copper alloy with fibrous structure reinforced by high density, multi-scale nano-precipitates and dislocation. *Materials Science & Engineering A,* 2022, 846: 143283.[DOI: 10.1016/j.msea.2022.143283]

[9] Zhang H, Fu H, Sun J, Jiang L, Zhu S, Xie J. Data-driven multi-process modeling and integrated design strategy for complex high-performance alloys. *Acta Materialia,* 2026, 302: 121648.[DOI: 10.1016/j.actamat.2025.121648]

[10] Yun P, Fu H, Zhang H, Sun J, Zhao M, Xie J. Rapid design of high-end copper alloy processes combining orthogonal experiments, machine learning, and Pareto analysis. *Journal of Materials Research and Technology,* 2025, 36: 1005-16.[DOI: 10.1016/j.jmrt.2025.03.119]

[11] Sun J, Fu H, Zhang H, Zhao M, Yun P, Xie J. Rapid design of processing parameters for Zero-Sample alloys via multi-acquisition-function Bayesian optimization. *Materials Science & Engineering A,* 2025, 944: 148904.[DOI: 10.1016/j.msea.2025.148904]

[12] Zhou Y, Yang J, Liu Y, et al. Ultrasonic vibration aging induces dislocation configuration evolution to achieve coordinated control of high strength and low residual stress of C70350 alloy strip. *Materials Science & Engineering A,* 2025, 922: 147655.[DOI: 10.1016/j.msea.2024.147655]

[13] Zhang H, Fu H, Zhu S, Yong W, Xie J. Machine learning assisted composition effective design for precipitation strengthened copper alloys. *Acta Materialia,* 2021, 215: 117118.[DOI: 10.1016/j.actamat.2021.117118]

[14] Y. Li, J. Xu, B. Guan, et al. Design of Cu-Ni-Si alloy with ultra-high strength and high conductivity based on machine learning model, *Journal of Materials Research and Technology* 42 (2026) 8572-84.[DOI: 10.1016/j.jmrt.2026.05.079]

[15] Li L, Liu G, Yu H, et al. A machine learning strategy to achieve strength-conductivity-ductility synergy of high-performance Cu-Ni-Co-Si alloys via rolling and aging process. *Journal of Materials Science & Technology,* 2026, 267: 184-97.[DOI: 10.1016/j.jmst.2025.12.040]

[16] Yang K, Wang Y, Guo M, et al. Recent development of advanced precipitation-strengthened Cu alloys with high strength and conductivity: A review. *Progress in Materials Science,* 2023, 138: 101141.[DOI: 10.1016/j.pmatsci.2023.101141]

[17] Zhang Y, Wang Z, Zhao S, et al. Effect of Cr addition on microstructure and properties of Cu-Ni-Co-Si-Mg alloys. *Journal of Alloys and Compounds,* 2026, 1050: 185684.[DOI: 10.1016/j.jallcom.2025.185684]

[18] Pan X, Xu J, Guan B, et al. Synergistic enhancement of strength and conductivity of Cu-Ni-Co-Si alloys by Ag addition. *Journal of Alloys and Compounds,* 2025, 1040: 183477.[DOI: 10.1016/j.jallcom.2025.183477]

[19] Deb K, Pratap A, Agarwal S, Meyarivan T. A fast and elitist multiobjective genetic algorithm: NSGA-II. *IEEE Transactions on Evolutionary Computation,* 2002, 6: 182-97.[DOI: 10.1109/4235.996017]

[20] Li R, Kang H, Chen Z, et al. A promising structure for fabricating high strength and high electrical conductivity copper alloys. *Scientific Reports,* 2016, 6: 20799.[DOI: 10.1038/srep20799]

[21] Zhao Z, Xiao Z, Li Z, Ma M, Dai J. Effect of magnesium on microstructure and properties of Cu-Cr alloy. *Journal of Alloys and Compounds,* 2018, 752: 191-7.[DOI: 10.1016/j.jallcom.2018.04.159]

[22] Zhou S, Lei Q, Yin J, et al. Effect of Si addition on the microstructure and mechanical properties of a Cu-Cr-Ag alloy with high strength and electrical conductivity. *Materials Science & Engineering A,* 2025, 934: 148310.[DOI: 10.1016/j.msea.2025.148310]

[23] Qin L, Zhou T, Jiang X, et al. Microstructure and properties of Cu-Ni-Co-Si-Cr-Mg alloy by multistage thermomechanical treatment. *Transactions of Nonferrous Metals Society of China,* 2023, 33: 3739-55.[DOI: 10.1016/S1003-6326(23)66367-8]

[24] He Z, Lin D, Lau T, Wu M. Gradient Boosting Machine: A Survey. (n.d.).[DOI:10.48550/arXiv.1908.06951]

[25] Xu S, Yang K, Chen H, Tan J, Gao Y. Negative hypervolume improvement assisted infill criterion for multi-objective efficient global optimization and its applications. *Swarm and Evolutionary Computation,* 2025, 99: 102190.[DOI: 10.1016/j.swevo.2025.102190]

[26] De Ville B. Decision trees. Wiley Interdisciplinary Reviews: Computational Statistics, 2013, 5: 448-55.[DOI: 10.1002/wics.1278]

[27] Zhang X, Wu H. Hesitant fuzzy linguistic Mahalanobis distance-based TOPSIS method for evaluating regional green development levels. *Applied Soft Computing,* 2025, 173: 112920.[DOI: 10.1016/j.asoc.2025.112920]

[28] Rumelhart DE, Hinton GE, Williams RJ. Learning representations by back-propagating errors. 1986.[DOI: 10.1038/323533a0]

[29] Breiman L. Stacked regressions. *Machine Learning,* 1996, 24: 49-64.[DOI: 10.1007/BF00117832]

[30] Cortes C, Vapnik V. Support-vector networks. *Machine Learning,* 1995, 20: 273-97.[DOI: 10.1007/BF00994018]

[31] Chen T, Guestrin C. XGBoost: A Scalable Tree Boosting System. In: Proceedings of the 22nd ACM SIGKDD International Conference on Knowledge Discovery and Data Mining. San Francisco, CA, USA: ACM; 2016: 785-94.[DOI: 10.1145/2939672.2939785]

[32] Li YH, Chen SF, Wang SW, Song HW, Zhang SH. Coarsening mechanism of over-aged δ-Ni_2Si nanoscale precipitates in Cu-Ni-Si-Cr-Mg alloy. *Materials Characterization,* 2024, 209: 113693.[DOI: 10.1016/j.matchar.2024.113693]

[33] Qin Z, Zhao H, Zhang S, et al. Design of high performance Cu-Ni-Si alloys via a multiobjective strategy based on machine learning. *Materials Today Communications,* 2024, 39: 108833.[DOI: 10.1016/j.mtcomm.2024.108833]

[34] Fu H, Yin Y, Zhang Y, Zhang M, Yun X. Enhancing the comprehensive properties of as-cast Cu-Ni-Si alloys by continuous extrusion combined with subsequent thermomechanical treatment. *Materials & Design,* 2022, 222: 111033.[DOI: 10.1016/j.matdes.2022.111033]

[35] Shan Y, Zhang C, Zhang Y, et al. Influence of different rolling passes and deformation amounts on the microstructure evolution and strengthening mechanism of Cu-Ni-Si alloy. *Journal of Materials Research and Technology,* 2024, 33: 3205-20.[DOI: 10.1016/j.jmrt.2024.10.035]

[36] Monzen R, Watanabe C. Microstructure and mechanical properties of Cu-Ni-Si alloys. *Materials Science & Engineering A,* 2008, 483-4: 117-9.[DOI: 10.1016/j.msea.2006.12.163]

[37] G.I. Taylor, The use of flat-ended projectiles for determining dynamic yield stress I. Theoretical considerations, *Proc. R. Soc. Lond. A Math. Phys. Sci.* 194 (1948) 289-99,[DOI: 10.1098/rspa.1948.0081]

[38] W.N. Liao, X.F. Liu, Y.H. Yang, Relationship and mechanism between double cold rolling-aging process, microstructure and properties of Cu-Ni-Si alloy prepared by two-phase zone continuous casting, *Mater. Sci. Eng.,* A 797 (2020) 140148,[DOI: 10.1016/j.msea.2020.140148]

[39] Lundberg SM, Lee SI. A Unified Approach to Interpreting Model Predictions. (n.d.).[DOI: 10.48550/arXiv.1705.07874]

[40] Freudenberger J, Kauffmann A, Klauß H, Marr T, Nenkov K, Sarma VS, Schultz L. Studies on recrystallization of single-phase copper alloys by resistance measurements. *Acta Materialia,* 2010, 58: 2324-9.[DOI: 10.1016/j.actamat.2009.12.018]

[41] Yasi JA, Hector LG, Trinkle DR. First-principles data for solid-solution strengthening of magnesium: from geometry and chemistry to properties. *Acta Materialia,* 2010, 58: 5704-13.[DOI: 10.1016/j.actamat.2010.06.045]

[42] Huang JZ, Xiao Z, Dai J, et al. Microstructure and properties of a novel Cu-Ni-Co-Si-Mg alloy with super-high strength and conductivity. *Materials Science & Engineering A,* 2019, 744: 754-63.[DOI: 10.1016/j.msea.2018.12.075]

[43] Jiang L, Wang CS, Fu HD, Shen J, Zhang ZH, Xie JX. Discovery of aluminum allys with ultra-strength and high-toughness via a property-oriented design strategy. *Journal of Materials Science & Technology,* 2022, 98: 33-43.[DOI: 10.1016/j.jmst.2021.05.011]

[44] Xue WL, Xie GL, Huang XX, et al. Achieving high strength and high-electrical-conductivity of Cu-Ni-Si alloys via regulating nanoprecipitation behavior through simplified process. *Journal of Materials Science & Technology,* 2025, 216: 121-9.[DOI: 10.1016/j.jmst.2024.07.039]

[45] Wang WC, Fu H, Zhang H, He X, Xie J. Simultaneous enhancement of mechanical and electrical properties of Cu-Ni-Si alloys via thermo-mechanical process. *Materials Science & Engineering A,* 2022, 838: 142815.[DOI: 10.1016/j.msea.2022.142815]

[46] Wang X, Xiao Z, Qiu WT, Li Z, Liu F. The evolution of microstructure and properties of a Cu-Ti-Cr-Mg-Si alloy with high strength during the multi-stage thermomechanical treatment. *Materials Science & Engineering A,* 2021, 803: 140510.[DOI: 10.1016/j.msea.2020.140510]

[47] Sitarama Raju K, Sarma VS, Kauffmann A, et al. High strength and ductile ultrafinegrained Cu-Ag alloy through bimodal grain size, dislocation density and solute distribution. *Acta Materialia,* 2013, 61: 228-38.[DOI: 10.1016/j.actamat.2012.09.053]

[48] X. Guo, L. Li, G. Liu, et al. Microstructure and properties of Cu-3Ti-0.3Cr-0.15Mg alloy designed via machine learning, *Materials Science and Engineering: A* 916 (2024) 147344.[DOI: 10.1016/j.msea.2024.147344]